Analysis of the magnetic coupling in a Mn(II)-U(V)-Mn(II) Single Molecule Magnet

Sourav Dey, Gopalan Rajaraman, Hélène Bolvin

▶ **To cite this version:**

Sourav Dey, Gopalan Rajaraman, Hélène Bolvin. Analysis of the magnetic coupling in a Mn(II)-U(V)-Mn(II) Single Molecule Magnet. Chemistry - A European Journal, 2022, 28 (68), pp.e202201883. 10.1002/chem.202201883 . hal-03766322

HAL Id: hal-03766322
https://hal.science/hal-03766322v1

Submitted on 31 Aug 2022

HAL is a multi-disciplinary open access archive for the deposit and dissemination of scientific research documents, whether they are published or not. The documents may come from teaching and research institutions in France or abroad, or from public or private research centers.

L'archive ouverte pluridisciplinaire **HAL**, est destinée au dépôt et à la diffusion de documents scientifiques de niveau recherche, publiés ou non, émanant des établissements d'enseignement et de recherche français ou étrangers, des laboratoires publics ou privés.

Analysis of the Magnetic Coupling in a Mn(II)-U(V)-Mn(II) Single Molecule Magnet

Sourav Dey[a], Gopalan Rajaraman[a]*, Hélène Bolvin [b]*

Abstract

[{Mn(TPA)I}{UO_2(Mesaldien)}{Mn(TPA)I}]I formula (here TPA = tris(2-pyridylmethyl)amine and Mesaldien = N,N'-(2-aminomethyl)diethylenebis(salicylidene imine)) reported by Mazzanti and coworkers (Chatelain et al. Angew. Chem. Int. Ed. **2014**, *53*, 13434) is so far the best Single Molecule Magnet (SMM) in the {3d-5f} class of molecules exhibiting barrier height of magnetization reversal as high as 81.0 K. In this work, we have employed a combination of ab initio CAS and DFT methods to fully characterize this compound and to extract the relevant spin Hamiltonian parameters. We show that the signs of the magnetic coupling and of the g-factors of the monomers are interconnected. The central magnetic unit $[U^{V}O_2]^+$ is described by a Kramers Doublet (KD) with negative g-factors, due to a large orbital contribution. The magnetic coupling for the {Mn(II)-U(V)} pair is modeled by an anisotropic exchange Hamiltonian: all components are ferromagnetic in terms of spin moments, the parallel component J_Z twice larger as the perpendicular one $J_\perp$. The spin density distribution suggests that spin polarization on the U(V) center favors the ferromagnetic coupling. Further, the $J_Z/J_\perp$ ratio, which is related to the barrier height, was found to correlate to the corresponding spin contribution of the g-factors of the U(V) center. This correlation established for the first time offers a direct way to estimate this important ratio from the corresponding g^S-values, which can be obtained using traditional ab initio packages and hence has a wider application to other {3d-5f} magnets. It is finally shown that the magnetization barrier height is tuned by the splitting of the $[U^{V}O_2]^+$ 5f orbitals.

Introduction

Single molecule magnets (SMMs) are of particular interest in the field of molecular magnetism due to their potential application in information storage and quantum computing [1]. The blocking barrier of magnetization reversal (U_{eff}) and blocking temperature (T_B, below which opening of hysteresis is observed) are considered to be figure of merit for the performance of a SMM [2, 3]. Recently groundbreaking results of achieving T_B as high as liquid nitrogen temperature in $[(Cp^{iPr5})Dy(Cp^*)]^+$ (Cp^{iPr5} = pentaisopropylcyclopentadienyl, Cp^* = pentamethylcyclopentadienyl) reveals that the magnetic anisotropy has reached its axial limit as further fine-tuning of the Ln-ligand interactions are not realistic [4, 5]. One way to circumvent this problem is to employ actinides that have diffused 5f orbitals exhibiting greater metal-ligand covalency - thanks to their extra radial node - compared to the 4f orbitals of the lanthanides [6, 7]. But the radioactivity of actinides makes them less explored than lanthanide and transition metal complexes.

Actinide, and in particular uranium complexes have the ability to be superior candidates for SMM due to their high anisotropy over the range of oxidation state and ability to mediate strong magnetic exchange with other metals [8]. The SMM behavior of U(III) complexes is inherent and well established [9, 10, 11, 12, 13, 14, 6, 7, 15, 16, 17, 18, 19, 20, 21]. On the other hand, U(V) complexes, though they possess only one unpaired electron, fair better due to a stronger ligand field arising from multiple metal-ligand characteristics with the donor atoms such as U=O [22, 23, 24, 25, 17]. The enhanced actinide-ligand covalency is also a disadvantage as even weaker ligands interact strongly yield large transverse anisotropy preventing achieving the Ising type of g-factors that are seen in lanthanides. Due to this factor, mononuclear actinide complexes exhibit stronger QTM, which often overcompensate the ground gained in magnetic anisotropy. However, if a strong exchange coupling is induced, this can substantially quench the tunneling, and this route leads to the birth of a handful of {3d-5f} magnets exhibiting very attractive barrier height/blocking temperatures [22, 26, 27].

[a]Department of Chemistry, Indian Institute of Technology Bombay Powai, Mumbai, Maharashtra, 400076, India

[b]Laboratoire de Chimie et Physique Quantiques, CNRS, Université Toulouse III, 118 route de Narbonne, 31062 Toulouse, France.

*e-mail addresses: rajaraman@chem.iitb.ac.in; bolvin@irsamc.ups-tlse.fr

Ab initio calculations based on Complete Active Space (CAS) principles have played an important role in modeling the magnetic anisotropy in lanthanide and actinide complexes. The modeling of one center lanthanide complexes is based on the splitting of the ground J [a] manifold by the crystal field [28, 29, 30], as the splitting of the ground manifold is similar to the thermal energy available at room temperature in most cases. In actinide complexes, the interaction with the ligands is more important and the ground J manifold might not be the good model space [31, 32, 33]. Even more, the An free ion is not the good starting point for the modeling of the actinyls, which must be considered as the basic unit perturbed by the equatorial ligands [34, 24, 35, 33]. In particular, for the $5f^1$ $[Np^{VI}O_2]^{2+}$ complex, which is isoelectronic to the $[U^{V}O_2]^{+}$ cation, the nature of the equatorial ligands completely dictates the magnetic properties.

The coupling between lanthanide centers is often described as an isotropic coupling using Lines model [36, 37], where the local properties are determined using ab initio calculations. Combined with a first principle description of the monomers, it allows to determine the value of the magnetic coupling J [38, 39, 40]. Considering only the couplings between two KDs, the fit can be performed using an Ising Hamiltonian [41]. This approach is valuable to calculate thermodynamic properties where the whole $2\mathsf{J}+1$ manifold of the free ion term is populated and estimates J values in good accordance against accurate High-Field EPR spectroscopy for a range of {3d-4f} dimers [42, 43]. The exchange coupling between two local J angular momenta may be expressed using the irreducible tensor algebra by a tensor which rank depends on the values of the local J [37]. In the present case, we limited the interaction to its second-order term since the local states are a KD doublet and a spin-only manifold. Furthermore, we neglected the antisymmetric contribution. Consequently, in the following, the exchange coupling is described by the tensor $\mathbf{J}$ [44, 45]

$$\begin{aligned} \hat{\mathcal{H}}^{AB} &= -\hat{\boldsymbol{S}}^{A}\,\mathbf{.}\,\mathbf{J}\,\mathbf{.}\,\hat{\boldsymbol{S}}^{B} \qquad (1)\\ &= -J_X\hat{S}_X^A\hat{S}_X^B - J_Y\hat{S}_Y^A\hat{S}_Y^B - J_Z\hat{S}_Z^A\hat{S}_Z^B \end{aligned}$$

where $\boldsymbol{S}^A$ and $\boldsymbol{S}^B$ are the local pseudo-spin operators. This simple form of Eq. 1 allows to model the interaction with a reduced number of parameters, whose physical interpretation is straighforward. Its applicability will be checked by comparing the response to a magnetic field with the model Hamiltonian to ab initio calculations. This coupling can be determined using EPR [46, 40, 47, 48].

There are few ab initio description of this coupling. CAS based methods are widely used to describe the crystal-field levels in mononuclear lanthanide/actinide complexes. For polynuclear systems the calculation of exchange couplings requires large active spaces which renders CAS based calculations extremely demanding. Furthermore, the calculation of exchange couplings requires the inclusion of dynamical correlation by multi-reference configuration interaction, perturbative methods being non reliable in those cases. This has been described using variational methods (DDCI) [49, 50], the local-density-fitted configuration-averaged Hartree–Fock (LDF-CAHF) method [51], Density-Matrix Renormalization Group (DMRG) method [52], and Density Functional Theory (DFT) [53]. DFT appears as an alternative tool to compute magnetic exchange coupling and to explore the electronic structure and magnetic properties of actinide-containing molecules, especially when the considered systems are very large [54].

A detailed understanding of the mechanism underlying the anisotropic coupling is of first importance in order to understand the anisotropy of polymetallic complexes. The coupling often reduces the SMM properties by creating desexcitations channels to the magnetization. It was shown that an anisotropic antiferromagnetic coupling should be the source for skyrmions [55]. This work is devoted to the detailed analysis of the anisotropic properties in a trinuclear exchange coupled {3d-5f} SMM [{Mn(TPA)I}{UO_2(Mesaldien)}-{Mn(TPA)I}]I (denoted [Mn–U–Mn], TPA = tris(2-pyridylmethyl) amine, Mesaldien = N,N-(2-aminomethyl)diethylenebis(salicylidene imine)), studied by Mazzanti and coworkers (see Figure 1) [26]. The Mn(II) centers with a high-spin $3d^5$ configuration have a half-filled shell: this leads to a simple electronic configuration that makes their description simpler and mostly spin-only non degenerate electronic state, with a negligible zero-field splitting. The central U(V) unit is highly anisotropic. The electronic and magnetic properties of actinyls are well described by CAS based methods including spin-orbit coupling and a perturbative description of the dynamical correlation [56, 57, 58, 59, 60, 34, 24, 61]. In this work, the magnetic monomers are first described using diamagnetic substitution, then the magnetic coupling is computed in the dimers and trimers using Configuration Interaction (CI) and DFT methods. This allows to discuss the spin Hamiltonian of the trimer and the subsequent properties.

Results and discussion

The [Mn–U–Mn] complex was synthesized and characterized in the group of Mazzanti [26]. It consists of two $[Mn(TPA)I]^{+}$ cations bound to the two oxo groups of the [UO_2(Mesaldien)] anion (see Fig-

[a] Note the typographic difference between J the total angular momentum quantum number and J the magnetic coupling parameter.

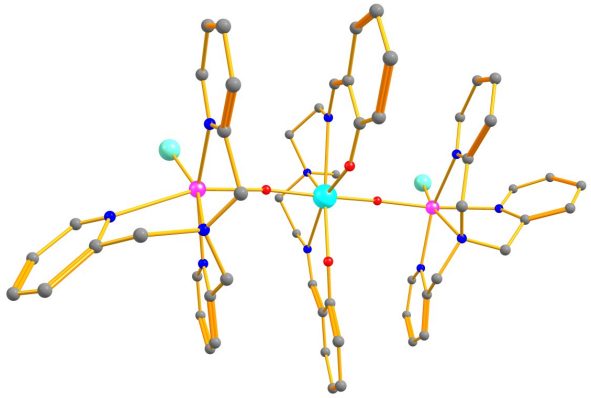

Figure 1: X-ray structure of [Mn−U−Mn] = [{Mn(TPA)I} {UO_2(Mesaldien)}{Mn(TPA)I}]I complex. Color code U: cyan, Mn: pink; I: aqua, O: red, N: blue, C: gray. H atoms are omitted for clarity.

ure 1). The U(V) atom is heptacoordinate with a slightly distorted pentagonal bipyramid geometry, with the two uranyl oxygen atoms O_{yl} and the five donor atoms of the Mesaldien^{2-} ligand in the equatorial plane. The transition metal centers are hexacoordinate, with a slightly distorted octahedral geometry defined by the four nitrogen atoms of the TPA ligand, one oxygen atom from the uranyl(V) group, and a coordinated iodide anion (see the SHAPE analysis in Table S1). The U=O bond length of 1.901 Å denotes a slight lengthening due to charge donation to the Mn(II) atom and the Mn−O_{yl} of 2.055 Å is significantly shorter than in equivalent complexes. The complex is almost linear, with a M−U−M angle of 173.77°, the deviation from linearity is due to intramolecular hydrogen bonds between the protons on the TPA ligand and the oxygen atoms of the Mesaldien^{2-} ligand. The magnetic susceptibility was measured and the high temperature χT curve was fitted by an Heisenberg Hamiltonian $\hat{\mathcal{H}}_S = -J\left(\boldsymbol{S}_{\mathrm{Mn1}} \cdot \boldsymbol{S}_{\mathrm{U}} + \boldsymbol{S}_{\mathrm{Mn2}} \cdot \boldsymbol{S}_{\mathrm{U}}\right)$ with a ferromagnetic coupling $J = 15$ cm^{-1} [b] and an isotropic g-factor for the U(V) center $g_{\mathrm{U}} = 1$. The complex exhibits a slow relaxation of magnetization in zero field with $U_{\mathrm{eff}} = 56.3$ cm^{-1}. It is reported to have the highest U_{eff} among all {3d-5f} complexes having a {M-O=U=O-M} (M = 3d metal ions) moiety.

The monomers

The Mn(II) cations have a $3d^5$ configuration and their high-spin ground state is an orbitally non-degenerate spin sextet. The zero-field splitting arises by spin-orbit coupling with the excited quartets at more than 20000 cm^{-1} and is less than 1 cm^{-1} (see Table S2 and 1). It will be neglected in the following and the Mn(II) centers described by a pure spin $S = 5/2$. The canonical orbitals are shown on Figure S3. They are similar for the two Mn(II) centers, and characteristic for an octahedral symmetry: the three t_{2g}-like orbitals split by 500 cm^{-1}, the e_g-like orbitals by 2000 cm^{-1} and the gap between the two groups is 6000 cm^{-1}.

[b] Note the difference of convention of the Heisenberg Hamiltonian with ref. [26].

Table 1: SO-CASSCF energies and zero-field splitting parameters (cm^{-1}) of the Mn(II) monomers.

	[Mn_1−U^{VI}]		[U^{VI}−Mn_2]	
	CAS (5,5)	CAS (5,10)	CAS (5,5)	CAS (5,10)
KD1	0	0.0	0.0	0
KD2	0.4	0.5	0.4	0.5
KD3	1.2	1.3	1.3	1.4
KD4	26701	24685	26278	24228
KD5	26704	24687	26281	24230
D [a]	0.20	0.21	0.21	0.23
E [a]	0.02	0.02	0.02	0.02

a: deduced from the three first KDs with spin Hamiltonian $\hat{\mathcal{H}}_S = D\left(S_Z^2 - \frac{1}{3}S(S+1)\right) + E\left[S_X^2 - S_Y^2\right]$ and S=5/2.

Table 2: Energies (cm^{-1}) of the U(V) monomers from spin-orbit calculations.

	[Zn−U−Zn]	[Zn−U−Zn]$_{\mathrm{mod}}$			
	CAS(1,6)	CAS(1,6)		RAS(13,18)	
	SCF	SCF	PT2	SCF	PT2
KD1	0	0	0	0	0
KD2	1124	1007	774	918	610
KD3	6486	6443	6296	6363	6214
KD4	9034	8973	8928	8844	8751
KD5	11658	11595	12036	11906	11378
KD6	14481	14420	14861	14636	14175

The uranyl group $[U^{V}O_2]^+$ is isoelectronic to the neptunyl $[Np^{VI}O_2]^{2+}$ with a $5f^1$ configuration. The magnetic properties of the latter are very sensitive to the nature of the equatorial ligands [24, 61]. The four f_δ are non-bonding to the O_{yl} atoms, while the f_π and f_σ are strongly destabilized, forming anti-bonding orbitals. In the ground state, the single electron lies in the f_δ or f_φ orbitals, and magnetic properties are determined by the composition of the ground KD in terms of those orbitals. The canonical orbitals of the [Zn−U−Zn]$_{\mathrm{mod}}$ complex are shown in Figure 2. The two f_δ orbitals are the lowest ones with a splitting of 400 cm^{-1}, followed by the two f_φ at 2000 and 4000 cm^{-1}, and finally the two f_π orbitals, almost degenerate at 6700 cm^{-1}. This scheme is usual for actinyls with equatorial ligands: the two former being involved in π interaction with the equatorial ligands, the two next in σ interactions and the two latter in π interaction with the two oxo groups, all those interactions being anti-bonding. The f_δ and f_φ orbitals have four-fold and three-fold symmetries along the U−O_{yl} axis, respectively, while the equatorial ligand is five-fold, but irregular. The two oxygen atoms are closer to the U(V) center than the three nitrogen ones (2.25 vs 2.61 Å). Consequently, $f_{\delta 2}$ is slightly more destabilized than $f_{\delta 1}$ because it interacts with the oxy-

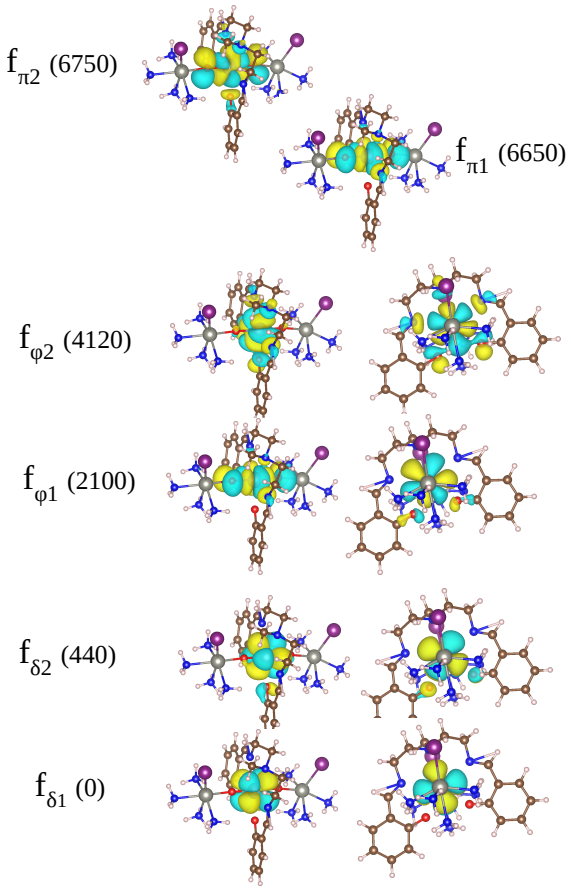

Figure 2: Canonical orbitals and energies (in parentheses, cm^{-1}) from SF-CASSCF of $[Zn-U-Zn]_{mod}$. Two perspectives are shown for the 4 lowest ones. Isovalue: 0.01 au.

gen atoms of the Mesaldien ligand. The splitting between $f_{\varphi 2}$ and $f_{\varphi 1}$ arises for the same reasons.

The energies of the U(V) monomer are given in Tables S3 and 2. The simplified $[Zn-U-Zn]_{mod}$ complex gives energies close to the $[Zn-U-Zn]$ complex. The magnetic orbitals in the complex are slightly perturbed as compared to the free $[U^{V}O_2]^{+}$, and are denoted according to the linear parentage: $|m_l|$ the value of $\hat{l}_Z$ for the orbitals and $|m_j|$ the value of $\hat{j}_Z$ for the spinors. The main effect of the equatorial ligands is to lift the degeneracy of the orbitals, the two f_δ by 700 cm^{-1} and the two f_φ by more than 2000 cm^{-1}. The states are labeled after the single occupied orbital (spin-orbit free) or spinor (spin-orbit). The ground spin-free state is of $^2\Delta_1$ parentage, with the single electron in the lowest $f_{\delta 1}$ orbital. The lowest excited state, at 700 cm^{-1}, is of $^2\Delta_2$ parentage, with the single electron in the $f_{\delta 2}$ orbital. The next excited states are of $^2\Phi$ parentage. In the $[U^{V}O_2]^{+}$ free ion, the spin-orbit coupling splits the $^2\Delta$ state according to $\Omega = |M_J|$ the value of $\hat{J}_Z$ in $\Delta_{5/2}$ and $\Delta_{3/2}$. In our complex, the composition of the ground KD is close to $\Delta_{3/2}$, ensued from the coupling between the two $^2\Delta$ components, whatever the level of calculation (see Table S6). The next KDs arise from the mixing between $^2\Delta$ and $^2\Phi$ manifolds. KD2 lies between 600 and 1100 cm^{-1}, depending on the level of calculation. The main effect of correlation is to lower the energy of $^2\Phi_1$ from 2000 to 1300 cm^{-1}. But this does not affect the ground KD, since of $\Omega = 3/2$ linear parentage, and the spin-orbit free $^2\Phi$ free-ion state spits in $\Phi_{5/2}$ and $\Phi_{7/2}$ by spin-orbit.

As a consequence, the ground KD can be modeled in the Δ space, as proposed in Section S2.2 [24]. The key parameter is the splitting by the equatorial ligands of the spin-orbit free $^2\Delta$ state in $^2\Delta_1$ and $^2\Delta_2$. The larger this splitting, the more quenched the orbital contribution. If the two δ orbitals are degenerate, the g-tensor is axial with a negative g_Z value. On the opposite, with an extremely large gap, only the $^2\Delta_1$ state contributes and as a pure spin doublet, it has an isotopic g tensor equals to $g_e = 2$. The present case is an intermediate regime, with a splitting of 700 cm^{-1} leading to relative weights of 60% and 30% for $^2\Delta_1$ and $^2\Delta_1$ and the orbital contribution is partially quenched. Ab initio g-factors are given in Table S5 in ESI. Since the composition of the ground KD in terms of spin-orbit free states barely depends on correlation, so do the g-factors. $g_\parallel^A$ and $g_\perp^A$ equal 1.6 and 0.5. g_X and g_Y are almost equal, as expected from $\mathcal{D}_{5h}$ symmetry, and will be considered to be equal in the following. The parallel spin and orbital contributions are in good accordance with Eqs. S2, with an orbital contribution about twice the spin one, and with opposite sign, leading to a negative value for $g_\parallel$. But Eqs. S2 predict a vanishing orbital contribution to the equatorial $g_\perp^L$, while the *ab initio* value is by far non zero, and even larger than the spin one. This might be due to the small weights of the ground KD on the $^2\Phi$ and $^2\Pi$ states. The sign of $g_\perp$ is undetermined, since only the product $g_X g_Y g_Z$ has a physical significance [62, 63]. The sign of $g_\perp^S$ can be assigned by switching off gradually the spin-orbit coupling: at the spin-free limit, all values equal to 2, by continuity $g_\perp^S$ is positive, and consequently, $g_\perp$ negative. In the following, we will keep this choice, keeping in mind its arbitrariness. The magnetic U(V) center will be modeled by a unique KD, with g-factors g_Z = -1.6 and $g_X = g_Y$ = -0.5.

The Natural Spin Orbitals (NSOs) correspond to the natural orbitals issued from the spin magnetization for a given direction of the external magnetic field as defined in references [24, 64, 65]. They allow to vizualize the orbitals contributing to the spin density, for a given quantification axis. NSOs with a positive (negative) population participate to the spin density with an α (β) spin for this quantification axis. The NSOs of the ground KD issued from the CASSCF and RASSCF calculations are represented in Figures S4 and S5, respectively and the corresponding spin magnetization densities are

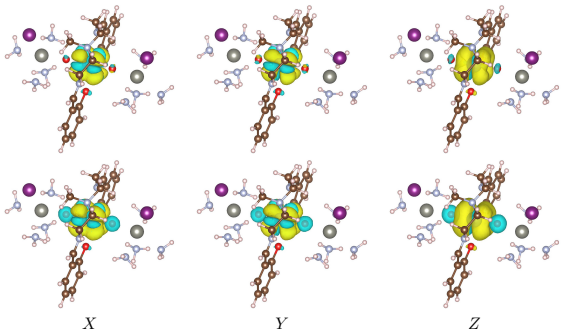

Figure 3: Spin density of the ground KD of the $[\mathrm{Zn-U-Zn}]_{\mathrm{mod}}$ complex, for the principal directions of the g tensor, from SO-CASSCF (above) and SO-RASSCF (below). Isovalue = 0.0002 e/bohr^{-3}.

shown in Figure 3. As shown in Section S2.2 of the SI, the decomposition of the two Kramers partners in their α and β components depends on the direction of the quantification axis, and consequently, of the applied magnetic field. Along both X and Z directions, f_{δ_1} and f_{δ_2} are NSOs with respective populations 0.6 and 0.3 (see Eqs. S4 and S7). But along Z, f_{δ_1} and f_{δ_2} orbitals appear both with a positive spin density, those contributions are additive and integrate to a large value, leading to an important longitudinal g-factor. Along X, f_{δ_1} and f_{δ_2} orbitals appear with opposite spins, and the spin density alternates with lobes of opposite signs: this integrates to a smaller value than in the Z direction. With both SO-CASSCF and SO-RASSCF, the NSOs correspond well to this model. The increase of the active space with orbitals of the oxo groups in RASSCF allows a better description of the correlation in these bonds, the main effect being the spin polarization [66, 67, 68, 69]. In the ground spin-orbit free $^2\Delta_1$ state, the Mulliken spin densities on the U and O_{yl} atoms are 0.9967 and 0.0005 with CASSCF, the spin density is positive on the oxo groups, since only spin delocalization is introduced. They become 1.0276 and -0.0154 with RASSCF, due to spin polarization. With spin-orbit coupling, there is a small amount of negative spin density, due to the coupling of the Δ states with the Π ones with opposite spin.

The trimer

The trimer consists of the $[UO_2]^+$ unit (denoted A) in the center, coupled to two Mn(II) centers (denoted B and C). Monomer A is the $[UO_2]^+$ unit, restricted to its ground KD, is described by a pseudo-spin $\mathbb{S}^A = 1/2$, the tensor $\mathbf{g}^A$ and its principal values $g_X^A = g_Y^A = g_\perp^A$ and g_Z^A.

$$\begin{aligned}\hat{\mathcal{H}}^A &= \mu_B \boldsymbol{B} \cdot \mathbf{g}^A \cdot \hat{\boldsymbol{S}}^A \\ &= \mu_B \left(g_X^A B_X \hat{S}_X + g_Y^A B_Y \hat{S}_Y + g_Z^A B_Z \hat{S}_Z \right) \end{aligned} \quad (2)$$

Monomers B and C are described by a pure spin $S^B = 5/2$ with a negligible zero-field splitting due to the half-shell structure. The spin Hamiltonian reduces to the isotropic Zeeman term

$$\hat{\mathcal{H}}^{B/C} = \mu_B g_e \boldsymbol{B} \cdot \hat{\boldsymbol{S}}^{B/C} \quad (3)$$

The coupling between the two magnetic centers is described by the anisotropic coupling Hamiltonian of Eq. 1. By symmetry, $J_X = J_Y = J_\perp$ and

$$\begin{aligned}\hat{\mathcal{H}}^{AB} &= -J_\perp \left(\hat{S}_X^A \hat{S}_X^B + \hat{S}_Y^A \hat{S}_Y^B \right) - J_Z \hat{S}_Z^A \hat{S}_Z^B \\ &= -J \, \hat{\boldsymbol{S}}^A \cdot \hat{\boldsymbol{S}}^B + D \left(\hat{S}_Z^A \hat{S}_Z^B \right. \\ &\quad \left. -\frac{1}{2} \hat{S}_X^A \hat{S}_X^B - \frac{1}{2} \hat{S}_Y^A \hat{S}_Y^B \right) \end{aligned} \quad (4)$$

with $J = (2J_\perp + J_Z)/3$ and $D = 2/3(J_\perp - J_Z)$. We suppose the principal axes frame (PAF) of $\mathbf{J}^{AB}$ and $\mathbf{g}^A$ to be identical.

We started by studying the dimers, and as a first example, the coupling between two KDs, $\mathbb{S}^A = 1/2$ and $\mathbb{S}^B = 1/2$ as developped in Section S3.1.1. It appears that the zero-field energies of the dimer are not affected by the reversal of sign of two components, J_α and J_β . The response to an external magnetic field is unaffected by this change of sign, if one flips the sign of the corresponding g-factors on one of the site: either g_α^A and g_β^A, or g_α^B and g_β^B. By changing both g_α^A, g_β^A, g_α^B and g_β^B, one retrieves the original sign for J_α and J_β. This rule applies whatever the values of $\mathbb{S}^A$ and $\mathbb{S}^B$ are. As depicted in Table S7, a ferromagnetic interaction ($J > 0$) favors the states with parallel pseudo-spins, ++ or −−. With positive g factors, it corresponds to parallel magnetic moments. If one of the g is negative, + corresponds to a negative magnetic moment, and the favored state has opposite magnetic moments; this is equivalent to an antiferromagnetic coupling ($J < 0$) with positive g factors. It comes out that the fitting of the ab initio spectra is not sufficient to provide the sign of the coupling parameters, and is related to the sign of the corresponding g factors.

We then considered the dimers, built by replacing one Mn(II) by a diamagnetic Zn(II). A chemical model $[\mathrm{Mn-U-Zn}]_{\mathrm{mod}}$ was considered, where the cycles of the ligands are removed, and the coordination sphere of the Zn(II) center simplified (see Figure S2). The dimers were first described by SO-CASSCF, with the $3d$ and $5f$ active orbitals. The dynamical correlation is further described, performing a RASSCF calculation which includes the bonding and antibonding σ and π orbitals of the yle bond. Finally, CI calulations were performed using the DDCI method. All results are given and discussed in details in Section S3.2.1 of the Supplementary Material. At the spin-free level, each of the six doublets of the $[U^V O_2]^+$ unit couples with the spin sextet of the Mn(II) center to form a septet and a quintet. For the Δ and Φ states, the septet lies below the corresponding quintet, which is the

Table 3: Spin Hamiltonian parameters (cm^{-1}) from the ab initio energies of the $[Mn-U-Zn]_{mod}$ dimer and from the experimental $\chi T = f(T)$ curve.

	fit energies $[Mn-U-Zn]_{mod}$ [a]				fit χT exp	
	CASSCF	RASSCF	CAS+S	DDCI2	[b]	[c]
$J_\perp$	4.7	6.0	9.6	10.0	30.9	22.5
J_Z	13.7	20.2	25.9	26.2	56.4	60.0
J	7.7	10.7	15.0	15.4	39.4	35.0
D	-6.0	-9.5	-10.8	-10.8	-17.0	-25.

a: fit of energies for the $[Mn-U-Zn]_{mod}$ dimer of Table S10 by spin Hamiltonian of Eq. 4. *b*: fit of the experimental $\chi T = f(T)$ curve using $g_\perp^A$ = -0.6 and g_Z^A = -1.57 and spin Hamiltonian of Eq. 5. *c*: fit with only J_{iso} using Eq. 9 with $g_X^{SA} = 0.6$; $g_Z^{SA} = 1.6$.

fingerprint of a ferromagnetic coupling. This coupling increases with correlation. With spin-orbit coupling, the 12 low lying states are fitted by the spin Hamiltonian, leading to parameters given in Table S11: J_Z is positive, while the sign of $J_\perp$ is undetermined. The values increase with the level of correlation, and $J_\perp$ is 2-3 times smaller than J_Z. It appears that the exchange coupling is largely reduced by the spin-orbit coupling as compared to the spin-free spectrum, by roughly a factor of 2. A similar effect was observed in the cerocene triple decker [49].

The comparison between the $M = f(B)$ and $\chi T = f(T)$ curves calculated from first-principles and deduced from the spin Hamiltonian with the parameters deduced at the same level of calculation, allows to assess that the spin Hamiltonian is able to reproduce the physics, and to assign the sign of the g factors of the central $[U^V O_2]^+$ unit, relatively to the J values. As developped in the Supporting Informations, it comes out that the J and g for the direction have opposite signs. In order to be coherent with the spin-free limit, the J components should be positive, leading to a ferromagnetic coupling in terms of spin densities, and the g_Z negative, due to the large orbital contribution, as shown in Section S2.2.

The trimer [Mn−U−Mn] was described at SO-CASSCF level, DFT using a broken-symmetry scheme and by a spin Hamiltonian. The CASSCF energies are given in Tables S12 and S13 of the ESI. At spin-orbit free level, each of the six spin doublets of the $[U^V O_2]^+$ unit couples with the two spin sextets to form one doducaplet, two docaplets, two octets, two sextets, two quartets and two doublets. Except for the Π states, the energy decreases with total spin, which denotes a ferromagnetic coupling. The simplified complex $[Mn-U-Mn]_{mod}$, where the cycles have been removed from the ligands (cf Figure S2), leads to energies similar to the whole one [Mn−U−Mn], except for the splitting between the two Δ manifolds which increases by more than 100 cm^{-1}, as for the dimer (cf Table S8), but not in the monomer (cf Table S3). The SO-CASSCF calculation provides the 36 KDs issued from the coupling between the two spin sextets of the Mn(II) centers and the ground KD of the $[U^V O_2]^-$ unit (cf Table S13). The overall splitting is 72 cm^{-1}, about twice the whole splitting in the dimer. There is a gap between KD21 and KD22. The g tensors go from axial to more or less equatorial from KD1 to KD21, and then from KD22 to KD36, from more or less equatorial to axial. KD36 has a larger g_Z than KD1.

The spin Hamiltonian for the trimer is the following

$$\hat{\mathcal{H}} = \hat{\mathcal{H}}^A + \hat{\mathcal{H}}^B + \hat{\mathcal{H}}^C + \hat{\mathcal{H}}^{AB} + \hat{\mathcal{H}}^{AC} + \hat{\mathcal{H}}^{BC} \quad (5)$$

where $\hat{\mathcal{H}}^A$ is given in Eq. 2, $\hat{\mathcal{H}}^B$ and $\hat{\mathcal{H}}^C$ in Eq. 3 and $\hat{\mathcal{H}}^{AC}$, $\hat{\mathcal{H}}^{AB}$ in Eq. 4. The coupling is considered to be equal with the two Mn(II) centers. $\hat{\mathcal{H}}^{BC}$ represents the Mn(II)-Mn(II) coupling and is described by a Heisenberg spin Hamiltonian $\hat{\mathcal{H}}^{BC} = -j\hat{\boldsymbol{S}}^B.\hat{\boldsymbol{S}}^C$. The spectra for different classes of parameters are shown on Figure S8. The SO-CASSCF spectrum of the trimer was fitted by this Hamiltonian (cf Table S14), leading to parameters very close to the dimer, with a positive value for J_Z, and undetermined sign for $J_X = J_Y$. The fit is improved with a small dissymmetry between J_X and J_Y which does not affect their average value and by adding a tiny positive magnetic direct coupling between the two Mn(II) centers, j = 0.06 cm^{-1}. As for the dimer, the response to the magnetic field with the spin Hamiltonian using the g-values of the monomer with different signs was compared to the ab initio curves (cf Figure S12). Again, negative $g_\perp$ and g_Z match better. This corresponds to positive spin contributions (see Section S2.2). Furthermore, the g-factors deduced from spin Hamiltonian compare well with the ab initio values which confirms that the spin Hamiltonian of Eq. 5 is an adequate model to describe the magnetic properties of the [Mn−U−Mn] complex.

The experimental χT curve is represented in Figure 4. The SO-CASSCF curve does not match the experimental one, the peak appears at too low temperatures. This is improved using the DDCI2 parameters, with a larger coupling. The fit proposed by Chatelain et al. [26] works only at high temperature and provides a too high and too narrow peak at low temperatures. We fitted the experimental $\chi T = f(T)$ curve with the two $J_\parallel$ and $J_\perp$ parameters, the g-factors fixed to their ab initio values, $g_\perp^A$ = -0.6 and g_Z^A = -1.57. One gets J_Z = 56.4 cm^{-1} and $J_\perp$ = 30.9 cm^{-1}, two-three times larger than the DDCI2 values. The experimental $M = f(B)$ curves are shown on Figure S12 and compared to those deduced from the spin Hamiltonian with the different sets of parameters. The set of parameters fitting the $\chi T = f(T)$ does not fit the $M = f(B)$ curves, leading to too small values of the magnetization. It is actually the SO-CASSCF curves which is in best accordance. We tried to fit jointly $\chi T = f(T)$ and

the $M = f(B)$ curves at different temperatures, but unsuccessfully. The axial of χT denotes a maximum, while the transverse component is smaller and increases smoothly with temperature; the two components converge to a plateau, where the contributions of the three centers are additive. The contribution for the U(V) center corresponds to a g-value of $\sqrt{2g_\perp^2 + g_\parallel^2}/3 = 1.03$, a value very close to the g_U from Chatelain et al. The ab initio g-factors are consequently in good accordance with the experimental data.

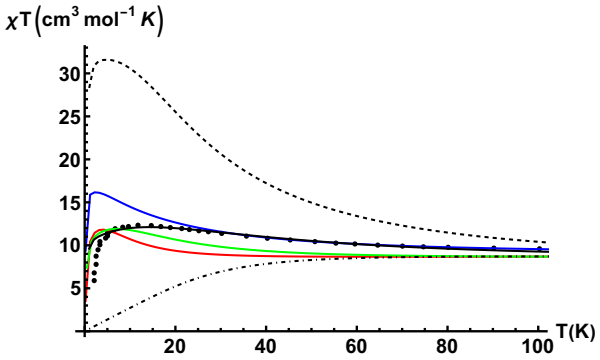

Figure 4: $\chi T = f(T)$ experimental, and deduced from Spin Hamiltonian with parameters from CASSCF (red), DDCI2 (green), from ref. [26] (blue) and fit of the χT curve (black; Z component dashed, $\perp$ component dot-dashed).

Broken-symmetry DFT provides magnetic couplings in good agreement with experimental data in {3d-4f} systems [70, 71]. The same approach was performed on the [Mn−U−Mn] complex using the B3LYP/TZVP set up. The calculations are performed without spin-orbit coupling and are modeled according to the broken-symmetry scheme for isotropic magnetic couplings. The high-spin and three broken-symmetry configurations were considered to estimate the three isotropic exchange coupling constants J^{AB}, J^{AC} and j. This leads to $J^{AB} = J^{AC} = 49.7$ cm^{-1} and $j = 0.5$ cm^{-1}. We remind here that those values are issued from calculations where the spin-orbit coupling is not included. As mentionned previously, the coupling reduces by roughly a factor of 2 with the spin-orbit coupling.

Spin densities of the four configurations are shown in Figure S13 and are compared to SF-RASSCF values for the dimer in Table S15 and Figure S6. In any case, there is a negative spin density on the bridging O_{yl} in the high-spin state. The magnetic orbital of the U(V) center is the same f_{δ_1} as in the ground state of CAS-based calculations. In all configurations, the spin density of the bridging O_{yl} atoms is opposite to the U(V) one; this shows the importance of the spin polarization of those atoms and that the magnetic unit is the $[U^VO_2]^+$ cation. Mulliken charges on the oxo oxygens are larger with DFT, which may explain the larger coupling with

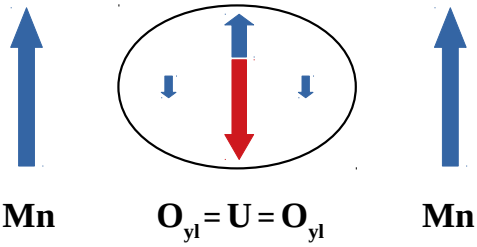

Figure 5: Magnetic scheme in the [Mn−U−Mn] trimer. Blue: spin, red: orbital.

this method, but the comparison should be performed with care, since the basis sets are different with the two methods.

The coupling in the dimer is finally described as a ferromagnetic coupling between a center with positive g-factors and an other with negative g-factors. The sign of the J-parameters denotes which state is favored in terms of pseudo-spins, while the sign of the g-factors denotes the relationship of the magnetic moment to the pseudo-spin. The coupling is found to be ferromagnetic because it was analyzed in terms of spin moments, with positive spin g-factors on the central unit. But, since the orbital contribution on the $[U^VO_2]^+$ unit is opposite to the spin one and dominant, this ferromagnetic coupling leads to opposite moments on the $[U^VO_2]^+$ and Mn(II) units. In the trimer, the moments of the two Mn(II) units are parallel, as a ferrimagnetic coupling scheme. We can summarize the coupling scheme by Figure 5: i) the coupling between the spin densities of the $[U^VO_2]^+$ and Mn(II) magnetic centers is ferromagnetic, in all directions, due to the spin polarization of the oxo bridging groups. ii) the anisotropy of the coupling is related to the anisotropy of the spin contribution of the **g** of the central magnetic $[U^VO_2]^+$ unit iii) the orbital contribution of the $[U^VO_2]^+$ unit being dominant and opposite to the spin one, the total magnetic moment of $[U^VO_2]^+$ is opposite to the ones of the two Mn(II) units. This is modeled by positive $J_\perp$ and J_Z and negative $g_\perp^A$ and g_Z^A parameters. iv) the overall magnetic scheme is ferrimagnetic.

The [Mn−U−Mn] complex exhibits a SMM behavior with a relaxation barrier U_{eff} of 81 K and exhibits an open magnetic hysteresis loop at temperatures below 3 K, with a significant coercive field of 1.9 T at 1.8 K. In lanthanide complexes, correlations can be found between the barrier U_{eff} and the energy of the first excited state, which is the sign of an Orbach relaxation process. In actinide complexes, the energy gaps are much larger, and this correlation is not as clear, which suggests that other relaxation pathways occur [72]. Anyhow, a ground state with an anisotropic magnetic moment, and excited states with anisotropic moments and large excitation energies are necessary to the SMM behavior. In Figure 6, the energy of the states is rep-

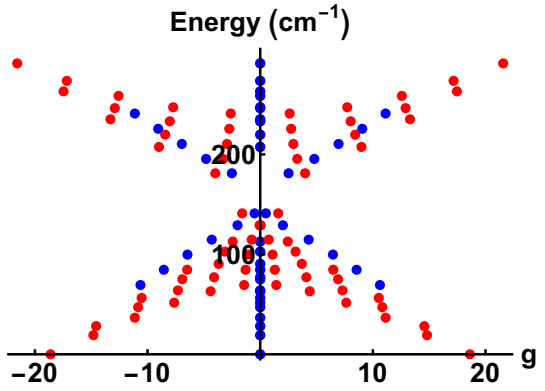

Figure 6: Energy (cm^{-1}) of the KDs of the trimer as a function of the g-factors; red: g_Z, blue $g_\perp$. $g_\perp^A$ = -0.5, g_Z^A = -1.6, $J_\perp$ = 30.9 cm^{-1}, J_Z = 56.4 cm^{-1}.

resented as a function of the axial (red) and transverse (blue) g-factors, deduced from the spin Hamiltonian with the coupling parameters fitting the experimental χT. One notices that the perpendicular magnetic component is zero up to 80 cm^{-1} while the parallel component decreases, leading to an energy barrier close to the experimental U_{eff} value. In Section S4.3 of the Supplementary Material, this scheme is depicted for different sets of parameters. It comes out that the barrier appears when the coupling is close to an Ising Hamiltonian, with $J_\perp$ as small as possible. The sign of J_Z does not influe much and the anisotropy of the $\mathbf{g}^A$ tensor does not impact this scheme ; the magnetization barrier issued from electronic states arises essentially from the anisotropy of the magnetic coupling.

In the Mn(III)−M(III)−Mn(III)(M=Ru,Os) SMM complexes [73, 74], the ground KD is issued from an orbitally degenerate spin-free state; the coupling is orbitally-dependent and consequently anisotropic [75]. In the present case, the ground KD is issued from two spin-free states $^2\Delta_1$ and $^2\Delta_2$. These two states have the same coupling with the Mn(II) centers. When degenerate, the KD is the $\Delta_{3/2}$ of the $[U^VO_2]^+$ cation, with a pure axial g tensor with both orbital and spin contributions (see Eqs. S2 with $B = 0$). The spin density of the $[U^VO_2]^+$ unit is represented in Figure 3 (see as well Eqs. S5 and S5 and NSOs in Figure S5); along Z, the contributions of the two δ orbitals are additive, which leads to a non-zero g_Z^{SA}, while along X or Y, they have opposite signs and this leads to a zero value for $g_\perp^{SA}$. With a splitting of the two δ orbitals, the cancellation is only partial, $g_\perp^{SA}$ is non-zero, and with a very large gap, the g^{SA}-factors are isotropic. The magnetic interaction between two magnetic centers is based on local spin densities. The spin g-factors are directly related to the spin densities along the corresponding direction $\rho_\alpha^S(\boldsymbol{r})$ as

$$g_\alpha^{SA} = 4 \int \rho_\alpha^S(\boldsymbol{r}) \mathrm{d}\boldsymbol{r} \tag{6}$$

The two δ orbitals are of the same symmetry as the corresponding d_δ, and consequently have the same interaction with the Mn centers, in accordance with the $X \equiv Y$ symmetry. But the spin density is axially anisotropic. One can expect the coupling interaction in a given direction to depend on the amount of spin density in this direction: if the latter vanishes, the interaction should vanish. In Table 3, the $J_\perp/J_Z$ ratio is worth between 0.3 and 0.38, and 0.55 with the fitted parameters, while in Table S5, g_X^{SA}/g_Z^{SA} is worth 0.38. It suggests to express the anisotropy of the coupling in terms of the anisotropy of the local g-tensors, as it is usually performed, but in terms of the anisotropy of the spin g-tensors. In Eq. 1, the exchange coupling is described as an anisotropic interaction between pseudo-spins. The pseudo-spins are mathematical operators which allow to describe the anisotropy of the local magnetic moments through the g tensor. Those magnetic moments break down in orbital and spin contributions, as specified by the $\mathbf{g}^L$ and $\mathbf{g}^S$ tensors, respectively. Consequently, the spin magnetic moment of a magnetic unit is $\mathbf{g}^S \cdot \hat{\boldsymbol{S}}$. Since the anisotropy of the coupling arises from the anisotropy of the spin densities, we propose to model the coupling between two magnetic centers A and B with respective spin g tensors $\mathbf{g}^{SA}$ and $\mathbf{g}^{SB}$ by an isotropic interaction between the anisotropic spin moments

$$\hat{\mathcal{H}}^{AB} = -\frac{1}{4} J_{\text{iso}} \left(\mathbf{g}^{SA} \cdot \hat{\boldsymbol{S}}^A\right)^\dagger \cdot \left(\mathbf{g}^{SB} \cdot \hat{\boldsymbol{S}}^B\right) \tag{7}$$

The factor 1/4 is introduced in order to obtain the usual Heisenberg Hamiltonian in the case of two isotropic spin-only magnetic centers. In the case where the two local g-tensors have the same PAF, Eq. 7 becomes

$$\begin{aligned} \hat{\mathcal{H}}^{AB} &= -\frac{1}{4} J_{\text{iso}} \left(g_X^{SA} g_X^{SB} \hat{S}_X^A \hat{S}_X^B + g_Y^{SA} g_Y^{SB} \hat{S}_Y^A \hat{S}_Y^B \right. \\ &\quad \left. + g_Z^{SA} g_Z^{SB} \hat{S}_Z^A \hat{S}_Z^B \right) \end{aligned} \tag{8}$$

and in the present case

$$\begin{aligned} \hat{\mathcal{H}}^{AB} &= -\frac{1}{2} J_{\text{iso}} \left(g_\perp^{SA} \hat{S}_X^A \hat{S}_X^B + g_\perp^{SA} \hat{S}_Y^A \hat{S}_Y^B \right. \\ &\quad \left. + g_Z^{SA} \hat{S}_Z^A \hat{S}_Z^B \right) \end{aligned} \tag{9}$$

which is equivalent to Eq. S18 with $J_\perp = \frac{1}{2} J_{\text{iso}} g_\perp^{SA}$; $J_Z = \frac{1}{2} J_{\text{iso}} g_Z^{SA}$ and $J = \frac{1}{2} J_{\text{iso}} \left(2 g_\perp^{SA} + g_Z^{SA}\right)$. We applied this approach by fitting the experimental χT curve; as shown in the last column of Table 3, this leads to parameters rather close from the two-parameters fit. This approach allows to reduce the fitting of the experimental curve to one parameter, once the one-center anisotropic magnetic properties are known.

The barrier is related to the anisotropy of the coupling, which depends on the anisotropy of the spin

g-tensor. The composition of the ground KD is tuned by the f_δ splitting. While this splitting smoothly impacts the axial spin density, it determines the transverse one: the transverse spin density sums up to 0 in the case of no gap and to 2 when the gap becomes important. It shows that this energy gap between the two f_δ orbitals plays a key role in the anisotropic properties, not only by introducing a large orbital contribution in the case of no gap, but by quenching the transverse spin contribution, and consequently by quenching the transverse magnetic coupling. The f_δ splitting is related to the symmetry of the equatorial ligands of the $[U^VO_2]^+$ unit. The splitting will be the largest with ligand with a four-fold symmetry, one of the f_δ being in this case largely anti-bonding.

Conclusions

The large metal-ligand covalency and stronger anisotropy of actinides make it very attractive for SMMs over lanthanides. Furthermore, the strong magnetic exchange substantially quenches the tunnelling, as shown in several cases. Despite these advantages, actinide chemistry is less explored. This is essentially due to a lack of solid theoretical understanding of the design principles and various factors that contribute to a reduction in barrier heights/blocking temperature. This work proposes a detailed analysis of the anisotropic magnetic properties in a {3d-5f-3d} trimer. This analysis is based on CAS based and scalar DFT methods, and spin Hamiltonian. The two Mn(II) centers are half-filled $3d^5$ shell with spin-only isotropic magnetic properties. The unpaired electron of the central $[U^VO_2]^+$ unit is mostly borne by the two $5f_\delta$ orbitals; the ground KD has an axial g-tensor, with negative values, due to a large orbital contribution, opposite to the spin one. The coupling between the $[U^VO_2]^+$ unit and the two Mn(II) centers is ferromagnetic, due to a large spin polarization of the oxo groups. It is anisotropic, larger in the parallel direction than in the transverse one, and increases with correlation. The sign of the transverse coupling can only be determined relative to the sign of the transverse g-factors. The spin Hamiltonian fits well the 72 magnetic states calculated with SO-CASSCF, which validates the ability of the spin Hamiltonian to describe this system. The two coupling parameters were finally fitted on the χT curves, using the ab initio g-factors of the $[U^VO_2]^+$ unit, leading to values larger than those determined by CAS-based and DFT methods. But, the main contribution to the magnetic moment of the $[U^VO_2]^+$ unit is orbital, which is opposite to the spin one, leading to negative g-factors. It follows that the magnetic moments are opposite on Mn(II) and U(V) centers: the ferromagnetic interaction between the spin magnetic moments becomes a ferrimagnetic interaction for the total moments, due to the local Hund's rule on the central cation.

The magnetization barrier is deduced from the spin Hamiltonian. Supposing that the relaxation follow an Orbach relaxation scheme, it corresponds to the experimental value [76, 77, 78, 79]. It is related to the anisotropy of the coupling, but is not affected by the anisotropy of the central g-tensor. The ratio of the transverse and axial components of the coupling and of the spin g-factors of the central unit are close. One can expect the anisotropy of the coupling to arise from the anisotropy of the spin density. The transverse spin density sums up to zero when the two f_δ orbitals are degenerate. As a result, in order to increase the barrier, one should quench the transverse spin contribution of the $[U^VO_2]^+$ unit, which is tuned by the splitting between the f_δ orbitals. Due to the four-fold symmetry of the latter, the splitting is favored by equatorial ligands denoting the same symmetry. As a consequence, one should avoid four-fold equatorial ligands in order to increase the barrier.

The fitting of the magnetic response for complexes with anisotropic properties is difficult, even impractical, due to the large number of parameters. Thanks to the use of the local g-tensors determined from ab initio calculations, only the coupling is fitted. In lanthanide complexes, the coupling is reduced to only one parameter, when the ground J manifold is populated [38, 39, 40]. This was performed in this work by expressing the coupling Hamiltonian as an isotropic interaction between the spin magnetic moments, which are anisotropic. The new fit, with only one parameter, is in good accordance with the two-parameters fit.

To summarize (i) The g factors of the ground KD of the central anisotropic unit $[U^VO_2]^+$ are negative, due to a large orbital contribution opposite to the spin one. Further, due to strong U-ligand covalency, we show that this anisotropy originates due to splitting within the 5f orbitals, particularly between two 5f orbitals. This allows to offer a design principle to enhance the anisotropy via ligand tuning. (ii) Due to the large orbital contribution opposite to the spin one, even if the coupling is ferromagnetic in terms of spin densities, the interaction in terms of magnetic moments is ferrimagnetic. (iii) The anisotropy of this interaction is related to the anisotropy of the spin density of the U(V) unit. Therefore, the use of local spin contribution to the g-tensor extracted from ab initio calculations allows reducing the number of parameters to be fitted in this anisotropic case to only one parameter. Consequently, the method can be used to analyze the magnetic properties of any other 3d-5f SMM, what we will do in a close future. (iv) The magnetization barrier is related to the anisotropy of the coupling, not from the anisotropy in the g factors as seen in

the lanthanide SMMs. Thus for the design of actinide SMMs, one has to focus on enhancing this exchange coupling via suitable ligand and not the individual single-ion anisotropy.

Computational details

WFT calculations

Calculations were performed on the X-ray structures [26] or simplified structures: (see Section S1 for more details) i) the trimers, with three paramagnetic centers, either complete [Mn−U−Mn] (cf Figure 1) or truncated $[Mn-U-Mn]_{mod}$ in which the TPA and Mesaldien ligands are simplified (cf Figure S2). ii) the dimers obtained by diamagnetic substitution: one of the Mn(II) centers is replaced by a diamagnetic Zn(II) cation with a simplified coordination sphere. The Mn(II) and U(V) center are either with the original coordination sphere [Mn−U−Zn] or with simplified ligands $[Mn-U-Zn]_{mod}$ (cf Figure S2). iii) the monomers, with only one paramagnetic center. In the Zn−U−Zn complex, the two Mn(II) centers are replaced by diamagnetic Zn(II) cations with a simplified coordination sphere, and in $[Mn-U^{VI}]$ complexes, U(V) is replaced by the diamagnetic U(VI) and the other Mn(II) center is removed (cf Figure S1). Our earlier work suggests that such approach has negligible effect on anisotropic properties [50].

WFT calculations were performed using MOLCAS 7.8 program package [80]. Spin-free wave functions were generated by the state average complete active space self-consistent field (SF-CASSCF) method [81]. The DKH (Douglas Kroll Hess) Hamiltonian was used to account of relativistic effects [82] and Cholesky decomposition to reduce the computational cost of calculating two-electron integrals [83]. Dynamical correlation in the U(V) monomer was calculated with the CASPT2 method [84]: the 5p(U) and 5d(U) are included in the correlation space, since it was shown that they may impact the results [61]. In the dimers, dynamical correlation was calculated by Configuration Interaction (CI) calculations performed with the CASDI program [85]: CAS+S and DDCI2 [86]. If S_1 (S_3) is the space of the orbitals which are doubly occupied (unoccupied) in the CASCI (Complete Active Space Configuration Interaction) calculation and n_h (n_p) the number of allowed holes (particles) in S_1 (S_3), the CAS+S CI corresponds to $n_h \leq 1$ and $n_p \leq 1$ and DDCI2 space contains all the configurations satisfying $n_h + n_p \leq 2$. CI calculations for the $[Mn-U-Zn]_{mod}$ complex involved 118 electrons in 429 orbitals, with a CAS(6,9) using the orbitals of the septet. CAS+S CI corresponds to $n_h \leq 1$ and $n_p \leq 1$. The spin-orbit interaction was calculated as a state interaction by RASSI-SO module [87]. Spin-Orbit (SO) integrals are calculated using the AMFI (Atomic Mean-Field Integrals) approximation [88]. SO-CAS+S and SO-DDCI2 results were obtained by dressing the spin-orbit matrix obtained with CASSCF with the corresponding Spin-orbit Free (SF) energies. Both for the state average CASSCF and the spin-orbit state interaction, all magnetic states were considered. Parameters for the zero-field splitting spin Hamiltonian of the Mn(II) centers were computed with the SINGLE_ANISO code [89]. g-factors and their spin and orbital contributions were calculated according to ref. [90] and magnetic susceptibility to ref. [91]. Basis sets, active spaces and spin-orbit state interaction are detailed in Section S1.

DFT calculations

DFT calculations were carried out using the G09 suite [92] using the hybrid B3LYP exchange-correlation functional [93]. Quadratic convergence was used to get the most stable wave function. A quasi relativistic ECP with 60 core electrons (ECP60MWB) along with ECP60MWB_ANO basis set was employed for Uranium as this ECP is well established to give a numerical accuracy [94]. Basis sets of Ahlrichs TZVP quality were used for Mn, O and C atoms and SVP for H [95]. Since these calculations do not include the spin-orbit coupling, the exchange coupling is isotropic and the following Heisenberg Hamiltonian was considered

$$\hat{\mathcal{H}} = -J\hat{\boldsymbol{S}}^A \cdot \hat{\boldsymbol{S}}^B - J\hat{\boldsymbol{S}}^A \cdot \hat{\boldsymbol{S}}^C - j\hat{\boldsymbol{S}}^B \cdot \hat{\boldsymbol{S}}^C \qquad (10)$$

where $\hat{\boldsymbol{S}}^A$, $\hat{\boldsymbol{S}}^A$ and $\hat{\boldsymbol{S}}^A$ are the local spin operators with $S_A = 1/2$ and $S_B = S_C = 5/2$. We underline that $\hat{\boldsymbol{S}}^A$ acts as a real spin in Eq. 10 while it acts as a pseudo-spin in Eq. 1. For our calculations, four configurations were considered: one high-spin HS = Mn1↑-U↑-Mn2↑ and three broken-symmetry, BS1 = Mn1↓-U↑-Mn2↑, BS2 = Mn1↑-U↑-M2↓, BS3 = Mn1↑-U↓-Mn2↑. Using the broken symmetry approach developed by Noodleman [96], the two coupling parameters J and j were estimated using the non-spin projected formula [97]: $E_{BS1} - E_{HS} = E_{BS1} - E_{HS} = 3J + 15j$ and $E_{BS3} - E_{HS} = 6J$.

Data availability

The data that support the findings of this study are openly available in ZENODO at https://doi.org/10.5281/zenodo.6659929.

Acknowledgments

S.D. thanks the grant NanoX n° ANR-17-EURE-0009 in the framework of the "Programme des Investissements d'Avenir" for the financial support during his stay in Toulouse. This work was supported by the ANR under convention N°ANR-17-CE06-0010. G.R. thanks CSIR (01(2980)/19/EMR-II) for funding.

References

[1] R. Sessoli, D. Gatteschi, A. Caneschi, M. Novak, *Nature* **1993**, 141–143.

[2] A. Castro-Alvarez, Y. Gil, L. Llanos, D. Aravena, *Inorg. Chem. Front.* **2020**, *7*, 2478–2486.

[3] M. J. Giansiracusa, A. K. Kostopoulos, D. Collison, R. E. P. Winpenny, N. F. Chilton, *Chem. Commun.* **2019**, *55*, 7025–7028.

[4] F.-S. Guo, B. M. Day, Y.-C. Chen, M.-L. Tong, A. Mansikkamäki, R. A. Layfield, *Science* **2018**, *362*, 1400–1403.

[5] C. A. P. Goodwin, F. Ortu, D. Reta, N. F. Chilton, D. P. Mills, *Nature* **2017**, 439–442.

[6] C. A. P. Goodwin, F. Tuna, E. J. L. McInnes, S. T. Liddle, J. McMaster, I. J. Vitorica-Yrezabal, D. P. Mills, *Chem. Eur. J.* **2014**, *20*, 14579–14583.

[7] K. R. Meihaus, S. G. Minasian, W. W. Lukens, S. A. Kozimor, D. K. Shuh, T. Tyliszczak, J. R. Long, *J. Am. Chem. Soc.* **2014**, *136*, 6056–6068.

[8] J. van Leusen, M. Speldrich, P. Kögerler, *Magnetism of Actinide Coordination Compounds*, Springer International Publishing, Cham, **2019**, 391–410.

[9] J. D. Rinehart, J. R. Long, *J. Am. Chem. Soc.* **2009**, *131*, 12558–12559.

[10] J. D. Rinehart, K. R. Meihaus, J. R. Long, *J. Am. Chem. Soc.* **2010**, *132*, 7572–7573.

[11] M. A. Antunes, L. C. J. Pereira, I. C. Santos, M. Mazzanti, J. Mar¸calo, M. Almeida, *Inorg. Chem.* **2011**, *50*, 9915–9917.

[12] J. T. Coutinho, M. A. Antunes, L. C. J. Pereira, H. Bolvin, J. Marçaloa, M. Mazzanti, M. Almeida, *Dalton Trans* **2012**, *41*, 13568.

[13] F. Moro, D. P. Mills, S. T. Liddle, J. van Slageren, *Angew. Chem. Int. Ed.* **2013**, *52*, 3430–3433.

[14] M. A. Antunes, I. C. Santos, H. Bolvin, L. C. J. Pereira, M. Mazzanti, J. Marçaloa, M. Almeida, *Dalton Trans* **2013**, *42*, 8861.

[15] S. T. Liddle, J. van Slageren, *Chem. Soc. Rev.* **2015**, *44*, 6655–6669.

[16] J. J. Le Roy, S. I. Gorelsky, I. Korobkov, M. Murugesu, *Organometallics* **2015**, *34*, 1415–1418.

[17] S. G. McAdams, A.-M. Ariciu, A. K. Kostopoulos, J. P. Walsh, F. Tuna, *Coordin. Chem. Rev.* **2017**, *346*, 216–239.

[18] M. Spivak, K. D. Vogiatzis, C. J. Cramer, C. d. Graaf, L. Gagliardi, *J. Phys. Chem. A* **2017**, *121*(8), 1726–1733.

[19] S. Dey, G. Velmurugan, G. Rajaraman, *Dalton Trans.* **2019**, *48*, 8976–8988.

[20] S. Dey, G. Rajaraman, *Chem. Commun.* **2022**, *58*, 6817–6820.

[21] S. Dey, G. Rajaraman, *Inorg. Chem.* **2022**, *61*, 1831–1842.

[22] D. M. King, F. Tuna, J. McMaster, W. Lewis, A. J. Blake, E. J. L. McInnes, S. T. Liddle, *Angew. Chem. Int. Ed.* **2013**, *52*, 4921–4924.

[23] V. Mougel, L. Chatelain, J. Hermle, R. Caciuffo, E. Colineau, F. Tuna, N. Magnani, A. de Geyer, J. Pécaut, M. Mazzanti, *Angew. Chem. Int. Ed.* **2014**, *53*, 819–823.

[24] F. Gendron, D. Páez Hernàndez, F. P. Notter, B. Pritchard, H. Bolvin, J. Autschbach, *Chem. Eur. J.* **2014**, *20*, 7994.

[25] D. M. King, P. A. Cleaves, A. J. Wooles, B. M. Gardner, N. F. Chilton, F. Tuna, W. Lewis, E. J. L. McInnes, S. T. Liddle, *Nat. commun.* **2016**, *7*, 13773.

[26] L. Chatelain, J. P. S. Walsh, J. Pécaut, F. Tuna, M. Mazzanti, *Angew. Chem. Int. Ed.* **2014**, *53*, 13434–13438.

[27] L. Chatelain, F. Tuna, J. Pécaut, M. Mazzanti, *Dalton Trans.* **2017**, *46*, 5498–5502.

[28] L. Ungur, L. F. Chibotaru, *Chem. Eur. J.* **2017**, *23*, 3708–3718.

[29] L. Ungur, *Introduction to the electronic structure, luminescence, and magnetism of lanthanides*, Elsevier, Advanced Nanomaterials, **2018**, 1 – 58.

[30] J. Jung, M. A. Islam, V. L. Pecoraro, T. Mallah, C. Berthon, H. Bolvin, *Chem. Eur. J.* **2019**, *25*, 15112–15122.

[31] F. P. Notter, H. Bolvin, *J. Chem. Phys.* **2009**, *130*, 184310.

[32] D. Páez Hernàndez, H. Bolvin, *J. Electron. Spectrosc. Relat. Phenom.* **2014**, *194*, 74.

[33] M. Autillo, M. A. Islam, J. Jung, J. Pilmé, N. Galland, L. Guerin, C. Berthon, C. Tamain, H. Bolvin, *Phys. Chem. Chem. Phys.* **2020**, *22*, 14293–14308.

[34] F. Notter, S. Dubillard, H. Bolvin, *J. Chem. Phys.* **2008**, *128*, 164315.

[35] F. Gendron, B. Pritchard, H. Bolvin, J. Autschbach, *Inorg. Chem.* **2014**, *53*, 8577–8592.

[36] M. E. Lines, *J. Chem. Phys.* **1971**, *55*, 2977.

[37] N. Iwahara, L. F. Chibotaru, *Phys. Rev. B* **2015**, *91*, 174438.

[38] L. F. Chibotaru, L. Ungur, A. Soncini, *Angew. Chem. Int. Ed.* **2008**, *120*, 4194–4197.

[39] C. Y. Chow, H. Bolvin, V. E. Campbell, J. W. Guillot, R. Kampf, W. Wernsdorfer, F. Gendron, J. Autschbach, V. Pecoraro, T. Mallah, *Chem. Sci.* **2015**, *6*, 4148.

[40] E. Moreno Pineda, N. F. Chilton, R. Marx, M. Dörfel, D. O. Sells, P. Neugebauer, S. D. Jiang, D. Collison, J. van Slageren, E. McInnes, R. E. P. Winpenny, *Nat. Commun.* **2014**, *5*, 5243.

[41] T. Han, M. J. Giansiracusa, Z.-H. Li, Y.-S. Ding, N. F. Chilton, R. E. P. Winpenny, Y.-Z. Zheng, *Chem. Eur. J.* **2020**, *26*, 6773–6777.

[42] T. Gupta, M. F. Beg, G. Rajaraman, *Inorg. Chem.* **2016**, *55*, 11201–11215.

[43] P. Comba, M. Enders, M. Großhauser, M. Hiller, R. Klingeler, C. Koo, D. Müller, G. Rajaraman, A. Swain, M. Tavhelidse, H. Wadepohl, *Chem. Eur. J.* **2021**, *27*, 9372–9382.

[44] T. Moriya, *Phys. Rev.* **1960**, *120*, 91–98.

[45] P. M. Levy, *Phys. Rev.* **1964**, *135*, A155–A165.

[46] M. D. Walter, C. H. Booth, W. W. Lukens, R. A. Andersen, *Organometallics* **2009**, *28*, 698.

[47] M. J. Giansiracusa, E. Moreno-Pineda, R. Hussain, R. Marx, M. Martínez Prada, P. Neugebauer, S. Al-Badran, D. Collison, F. Tuna, J. van Slageren, S. Carretta, T. Guidi, E. J. L. McInnes, R. E. P. Winpenny, N. F. Chilton, *J. Am. Chem. Soc.* **2018**, *140*, 2504–2513.

[48] M. J. Giansiracusa, S. Al-Badran, A. K. Kostopoulos, G. F. S. Whitehead, E. J. L. McInnes, D. Collison, R. E. P. Winpenny, N. F. Chilton, *Inorg. Chem. Front.* **2020**, *7*, 3909–3918.

[49] F. Gendron, J. Autschbach, J. Malrieu, H. Bolvin, *Inorg. Chem.* **2019**, *58*, 581–593.

[50] F. Koprowiak, Dissertation, Université de Toulouse, Toulouse, **2017**.

[51] P. P. Hallmen, H.-J. Werner, D. Kats, S. Lenz, G. Rauhut, H. Stoll, J. van Slageren, *Phys. Chem. Chem. Phys.* **2019**, *21*, 9769–9778.

[52] C. Gould, K. McClain, D. Reta, J. Kragskow, D. Marchiori, E. Lachman, E. Choi, J. Analytis, R. Britt, N. Chilton, B. Harvey, J. Long **2022**, *375*, 198–202.

[53] B. Teyar, S. Boucenina, L. Belkhiri, B. Le Guennic, A. Boucekkine, M. Mazzanti, *Inorg. Chem.* **2019**, *58*, 10097–10110.

[54] L. Belkhiri, B. Le Guennic, A. Boucekkine, *Magnetochemistry* **2019**, *5*.

[55] S. Gao, H. D. Rosales, F. A. G. Albarracín, V. Tsurkan, G. Kaur, T. Fennell, P. Steffens, M. Boehm, P. Čermák, A. Schneidewind, E. Ressouche, D. C. Cabra, C. Ruegg, O. Zaharko, *Nature* **2020**, *586*, 37–41.

[56] L. Maron, T. Leininger, B. Schimmelpfennig, V. Vallet, J. L. Heully, C. Teichtel, O. Gropen, U. Wahlgren, *Chem. Phys.* **1999**, *244*, 195.

[57] Z. Zhang, R. M. Pitzer, *J. Phys. Chem. A* **1999**, *103*, 6880.

[58] L. Gagliardi, B. O. Roos, P.-A. Malmqvist, J. M. Dyke, *J. Phys. Chem. A* **2001**, *105*, 10602.

[59] K. Pierloot, E. van Besien, *J. Chem. Phys.* **2005**, *123*, 204309.

[60] I. Infante, E. Eliav, M. J. Vilkas, Y. Ishikawa, U. Kaldor, L. Visscher, *J. Chem. Phys.* **2007**, *127*, 124308.

[61] M. Autillo, M. A. Islam, J. Héron, L. Guérin, E. Acher, C. Tamain, M.-C. Illy, P. Moisy, E. Colineau, J.-C. Griveau, C. Berthon, H. Bolvin, *Chem. Eur. J.* **2021**, *27*, 7138–7153.

[62] L. Chibotaru, A. Ceulemans, H. Bolvin, *Phys. Rev. Lett.* **2008**, *101*, 033003.

[63] H. Bolvin, J. Autschbach, *Handbook of relativistic quantum chemistry*, Springer, Berlin, Kap. Relativistic methods for calculating Electron Paramagnetic Resonance (EPR) parameters, **2017**.

[64] F. Gendron, B. Pritchard, H. Bolvin, J. Autschbach, *Dalton Trans.* **2015**, 19886.

[65] F. Gendron, H. Bolvin, J. Autschbach, *Complete Active Space Wavefunction-Based Analysis of Magnetization and Electronic Structure*, Springer International Publishing, Cham, **2019**, 355–390.

[66] O. Kahn, *Molecular magnetism*, Wiley-VCH, New-York, **1993**.

[67] F. Lloret, G. De Munno, M. Julve, J. Cano, R. Ruiz, A. Caneschi, *Angew. Chem. Int. Ed.* **1998**, *37*, 135–138.

[68] I. Fernández, R. Ruiz, J. Faus, M. Julve, F. Lloret, J. Cano, X. Ottenwaelder, Y. Journaux, M. C. Muñoz, *Angew. Chem. Int. Ed.* **2001**, *40*, 3039–3042.

[69] H. Theil, C.-G. F. von Richthofen, A. Stammler, H. Bögge, T. Glaser, *Inorg. Chim. Acta* **2008**, *361*, 916–924.

[70] K. R. Vignesh, S. K. Langley, K. S. Murray, G. Rajaraman, *Chem. Eur. J.* **2017**, *23*, 1654–1666.

[71] L. Rosado Piquer, S. Dey, L. Castilla-Amorós, S. J. Teat, J. Cirera, G. Rajaraman, E. C. Sañudo, *Dalton Trans.* **2019**, *48*, 12440–12450.

[72] K. R. Meihaus, J. R. Long, *Dalton Trans.* **2015**, *44*, 2517–2528.

[73] J. Dreiser, K. S. Pedersen, A. Schnegg, K. Holldack, J. Nehrkorn, M. Sigrist, P. Tregenna-Piggott, H. Mutka, H. Weihe, V. S. Mironov, J. Bendix, O. Waldmann, *Chem. Eur. J.* **2013**, *19*, 3693–3701.

[74] S. K. Singh, G. Rajaraman, *Chem. Eur. J.* **2014**, *20*, 113–123.

[75] A. Palii, B. Tsukerblat, S. Klokishner, K. Dunbar, J. Clemente-Juan, E. Coronado, *Chem. Soc. Rev.* **2011**, *40*, 3130–3156.

[76] A. Lunghi, F. Totti, R. Sessoli, S. Sanvito, *Nat. Commun.* **2017**, *375*, 14620.

[77] L. Escalera-Moreno, J. J. Baldoví, A. Gaita-Ariño, E. Coronado, *Chem. Sci.* **2020**, *11*, 1593–1598.

[78] M. Briganti, F. Santanni, L. Tesi, F. Totti, R. Sessoli, A. Lunghi, *J. Am. Chem. Soc.* **2021**, *143*, 13633–13645.

[79] J. Kragskow, J. Marbey, C. Buch, J. Nehrkorn, M. Ozerov, S. Pilikkos, N. F. Chilton, *Nat. Commun.* **2022**, *13*, 825.

[80] F. Aquilante, L. De Vico, N. Ferré, G. Ghigo, P.-Å. Malmqvist, P. Neogrády, T. B. Pedersen, M. Pitonak, M. Reiher, B. Roos, M. Serrano-Andrés, M. Urban, V. Veryazov, R. Lindh, *J. Comput. Chem.* **2010**, *31*, 224.

[81] B. O. Roos, P. R. Taylor, P. E. M. Siegbahn, *Chem. Phys.* **1980**, *48*, 157.

[82] A. Wolf, M. Reiher, B. A. Hess, *J. Chem. Phys.* **2002**, *117*, 9215–9226.

[83] F. Aquilante, P.-Å. Malmqvist, T. B. Pedersen, A. Ghosh, B. O. Roos **2008**, *4*, 694–702.

[84] K. Andersson, P.-A. Malmqvist, B. O. Roos, A. J. Sadlej, K. Wolinski, *J. Phys. Chem.* **1990**, *94*, 5483.

[85] N. Benamor, D. Maynau, *Chem. Phys. Lett.* **1998**, *286*, 211.

[86] J. Miralles, J.-P. Daudey, R. Caballol, *Chem. Phys. Lett.* **1992**, *198*, 555.

[87] P.-A. Malmqvist, B. O. Roos, B. Schimmelpfennig, *Chem. Phys. Lett.* **2002**, *357*, 230.

[88] B. A. Hess, C. M. Marian, U. Wahlgren, O. Gropen, *Chem. Phys. Lett.* **1996**, *251*, 365.

[89] L. Chibotaru, L. Ungur, *J. Chem. Phys.* **2012**, *137*, 064112.

[90] H. Bolvin, *ChemPhysChem* **2006**, *7*, 1575.

[91] S. Vancoillie, F. Neese, L. Rulisek, K. Pierloot, *J. Phys. Chem. A* **2009**, *113*, 6149.

[92] M. J. Frisch, G. W. Trucks, H. B. Schlegel, G. E. Scuseria, M. A. Robb, J. R. Cheeseman, G. Scalmani, V. Barone, G. A. Petersson, H. Nakatsuji, X. Li, M. Caricato, A. V. Marenich, J. Bloino, B. G. Janesko, R. Gomperts, B. Mennucci, H. P. Hratchian, J. V. Ortiz, A. F. Izmaylov, J. L. Sonnenberg, D. Williams-Young, F. Ding, F. Lipparini, F. Egidi, J. Goings, B. Peng, A. Petrone, T. Henderson, D. Ranasinghe, V. G. Zakrzewski, J. Gao, N. Rega, G. Zheng, W. Liang, M. Hada, M. Ehara, K. Toyota, R. Fukuda, J. Hasegawa, M. Ishida, T. Nakajima, Y. Honda, O. Kitao, H. Nakai, T. Vreven, K. Throssell, J. A. Montgomery, Jr., J. E. Peralta, F. Ogliaro, M. J. Bearpark, J. J. Heyd, E. N. Brothers, K. N. Kudin, V. N. Staroverov, T. A. Keith, R. Kobayashi, J. Normand, K. Raghavachari, A. P. Rendell, J. C. Burant, S. S. Iyengar, J. Tomasi, M. Cossi, J. M. Millam, M. Klene, C. Adamo, R. Cammi, J. W. Ochterski, R. L. Martin, K. Morokuma, O. Farkas, J. B. Foresman, D. J. Fox, Gaussian 09 Revision A.01, **2016**, gaussian Inc. Wallingford CT.

[93] A. D. Becke, *J. Chem. Phys.* **1993**, *98*, 5648.

[94] D. Andrae, U. Haeussermann, M. Dolg, H. Preuss, *Theor. Chem. Acc.* **1990**, *77*, 123.

[95] A. Schäffer, C. Huber, R. Ahlrichs, *J. Chem. Phys.* **1994**, *100*, 5829.

[96] L. Noodleman, D. A. Case, A. Aizman, *J. Am. Chem. Soc.* **1988**, *110*, 1001–1005.

[97] E. Ruiz, J. Cano, S. Alvarez, P. Alemany, *J. Comput. Chem. 20*, 1391–1400.